Retrieval of Hydrometeor Profiles in Tropical Cyclones and Convection from Combined Radar and Radiometer Observations

HAIYAN JIANG* AND EDWARD J. ZIPSER

Department of Meteorology, University of Utah, Salt Lake City, Utah

(Manuscript received 31 March 2005, in final form 16 December 2005)

ABSTRACT

A retrieval algorithm is described to estimate vertical profiles of precipitation ice water content and liquid water content in tropical cyclones and convection over ocean from combined spaceborne radar and radiometer measurements. In the algorithm, the intercept parameter N_0s in the exponential particle size distribution for rain, snow, and graupel are adjusted iteratively to minimize the difference between observed brightness temperatures and simulated ones by using a simulated annealing optimization method. Sensitivity tests are performed to understand the effects of the input parameters. The retrieval technique is investigated using the Earth Resources (ER)-2 aircraft Doppler radar and Advanced Microwave Precipitation Radiometer data in tropical cyclones and convection. An indirect validation is performed by comparing the measured and retrieved 50-GHz (independent channel) brightness temperature. The global agreement shows not only the quality of the inversion procedure, but also the consistency of the retrieved parameters with observations. The direct validation of the ice water content retrieval by using the aircraft in situ microphysical measurements indicates that the algorithm can provide reliable ice water content estimates, especially in stratiform regions. In convective regions, the large variability of the microphysical characteristics causes a large uncertainty in the retrieval, although the mean difference between the retrieved ice water content and aircraft-derived ice water content is very small. The ice water content estimated by a radar-only empirical relationship is higher than those retrieved by the combined algorithm and derived by the aircraft in situ observations. The new combined algorithm contains information that should improve ice water content estimates from either radar-only or passive microwave–only measurements. An important caveat for this study is that it concerns *precipitation* estimates. In this paper, ice and liquid water content should be interpreted as *precipitation* ice and liquid water content.

1. Introduction

One of the main goals of the Tropical Rainfall Measuring Mission (TRMM) is to advance the objective of understanding the global energy and water cycles by providing four-dimensional distributions of latent heating over the global Tropics (Simpson et al. 1988; Kummerow et al. 2000). Tropical cyclones and convection are very important rainfall systems over the global Tropics and are a major component the energy and water budgets. The latent heat release in tropical cyclones provides heating and produces a warm-core structure, which is essential for the development and maintenance of the circulation of the storm. Directly related to latent heating, ice water content (IWC) and liquid water content (LWC) have implications on tropical cyclone intensity (Cecil and Zipser 1999; Rao and MacArthur 1994). Early numerical hurricane model simulations show that the ice-phase microphysics plays an important role in the evolution of the simulated hurricane (Lord et al. 1984).

Microwave remote sensing techniques for rainfall can be classified broadly into radar-only, radiometer-only, and combined radar–radiometer approaches based on the instruments to be used. By examining a 1-yr TRMM tropical cyclone database (Cecil et al. 2002), Jiang (2004) found that the TRMM version-5 radiometer-only 2A12 algorithm (Kummerow et al. 1996) obtains an unrealistic estimate of the vertical profile shape, and the TRMM version-5 radar-only 2A25 algorithm (Igu-

* Current affiliation: Joint Center for Earth Systems Technology, University of Maryland, Baltimore County, Baltimore, and NASA Goddard Space Flight Center, Greenbelt, Maryland.

Corresponding author address: Dr. Haiyan Jiang, NASA/GSFC, Code 613.1, Bldg. 33, Rm. C415, Greenbelt, MD 20771.
E-mail: jiang@agnes.gsfc.nasa.gov

chi et al. 2000; T. Iguchi 2002, personal communication) gives a big underestimate of the total amount of ice water content because of the particle size distribution (PSD) assumption.

Airborne and satellite-borne radar and radiometer on the same platform, such as TRMM and the Convection and Moisture Experiment (CAMEX), provide a very powerful tool to estimate IWC and LWC profiles in tropical precipitation systems. Recent studies demonstrate various ways in which the opportunities to estimate hydrometeor profiles and cloud characteristics improve by combining radar and radiometers (Olson et al. 1996; Marzano et al. 1999; Viltard et al. 2000; Grecu and Anagnostou 2002).

By combining radar and radiometer observations, the PSD parameters can be retrieved along with the hydrometeor profiles, which is the first advantage of a combined algorithm. Second, one of the biggest problems of emission-based radiometer algorithms is the determination of the freezing level (Wilheit et al. 1977, 1991; Kummerow et al. 2001; Jiang et al. 2006). By adding radar observations, the freezing level can be estimated by the radar brightband height in stratiform regions and extrapolated into neighboring convective regions, therefore minimizing uncertainties. Third, the convective–stratiform separation represents another big uncertainty of a radiometer-only algorithm, such as TRMM 2A12 (Kummerow et al. 2001). Although the rain-type classification by radar data is also subject to some uncertainties, the separation based on the 3D structure of the radar observation would definitely be better than that from the 2D radiometer observations. Fourth, a radiometer-only algorithm theoretically can give a good estimate of the integrated water content [ice water path (IWP), liquid water path (LWP)], but the radiometer observation is not enough to obtain the vertical shape of IWC and LWC because there are more independent variables within raining clouds than there are channels in the observing systems. Instead, radar can measure the vertical distribution of reflectivity. Therefore, a radar algorithm can give a reasonable vertical shape of the hydrometeor profiles. By combining these two observations, one can expect both a reasonable total amount of water content and a vertical shape of the profiles. For developing a fully physical retrieval algorithm, it is likely that combining radar and radiometer information will lead to more realistic profiles and more accurate estimates.

The TRMM standard combined radar–radiometer algorithm 2B31 (Haddad et al. 1997) uses an a priori probability density function of raindrop size distribution variables to retrieve rain-rate profiles from the radar and radiometer 10-GHz-channel measurements. An a priori cloud model database was applied in some combined algorithm studies (Olson et al. 1996; Marzano et al. 1999) to obtain both cloud and precipitation hydrometeor profiles in tropical convective systems. Among a few combined algorithms independent of cloud model output, Skofronick-Jackson et al.'s (2003) approach emphasizes high frequencies (>150 GHz) and cannot be implemented in TRMM satellite observations; Grecu et al. (2004, hereinafter GP) provide a combined technique that has been applied to TRMM observations, but use the same N_0 (one of the coefficients in PSD) for rain, snow, and graupel, and cannot retrieve a reasonable hydrometeor profile in the ice region, although its rain-rate retrieval is comparable with ground-based radar estimates.

In this paper, we develop a simple but comprehensive version of GP's technique by formulating and investigating a combined algorithm that uses different N_0 values for rain, snow, and graupel to estimate both IWC and LWC profiles consistent with both radar and radiometer observations. Only the oceanic background is considered in this algorithm. The precipitation microwave radar and radiometer at frequencies less than 85 GHz mainly detect precipitation-sized particles. The precipitation radar detects the backscattering of particles, while the microwave radiometer senses both the emission and scattering of particles. A nondimensional size parameter x is defined as

$$x \equiv \frac{2\pi r}{\lambda}, \tag{1}$$

where r is the radius of a spherical particle. Given the value of x, one can immediately determine whether scattering by the particle is likely to be significant and, if so, which broad scattering regime—Rayleigh, Mie, or geometric optics—is most applicable. For an ice sphere in the microwave band, when $x < 1.2$, the scattering coefficient is proportional to D^6 (D is the diameter of the particle), as in Rayleigh regime; when $1.2 < x < 6$, the relation between the scattering coefficient and particle diameter D is not monotonic, as in the Mie regime; when $x > 6$, the scattering coefficient is independent of D, as in the geometric optics regime (Jiang 2004). Therefore, cloud-sized particles are mainly in the Rayleigh regime for the microwave radar and radiometer. Here we define cloud (no significant fallout) particles as having a particle radius between ~0.1 and ~100 μm, while precipitation (significant fallout) particles have a radius between ~100 μm and ~6 mm. The contribution from cloud ice and liquid particles to the precipitation radar reflectivity and radiometer brightness temperature is very small relative to the contribution from pre-

cipitation-sized particles in the Rayleigh regime. Therefore, IWC and LWC in this paper should be interpreted as *precipitation* IWC and LWC. The detailed algorithm description is presented in section 2. Sensitivity tests about cloud IWC and LWC as well as other parameters will be performed in section 3. Section 4 is devoted to validating this algorithm by using independent aircraft in situ microphysical measurements and microwave radiometer measurements other than Advanced Microwave Precipitation Radar (AMPR) channels, and comparing the retrievals with radar-only, radiometer-only, and simplified GP estimates to understand the advantage and disadvantage of different methods. Section 5 contains conclusions.

2. Algorithm description

The combined radar–radiometer retrieval algorithm developed here uses radar reflectivity–derived hydrometeor profiles as input to a forward radiative transfer model (RTM) to retrieve N_0s by minimizing the differences between observed brightness temperatures and calculated ones iteratively. The plane-parallel microwave radiative transfer code used here was developed by Kummerow and Weinman (1988) and Kummerow et al. (1996). In this RTM, the PSD is assumed to be exponential,

$$N(D) = N_0 e^{-\lambda D}, \tag{2}$$

where D is the equivalent spherical particle diameter, N_0 is the intercept parameter, and λ is the slope parameter. In the combined algorithm, the iteratively adjusted parameters would be the coefficients N_{0r}, N_{0s}, and N_{0g} for rain, snow, and graupel, respectively, in (2). The slope parameter λ would be adjusted along with N_0 because λ can be determined by any two of the following three parameters: N_0, water content M, and radar reflectivity Z. Although the PSD is assumed to be exponential for the entire retrieval, the intercept parameter N_0 would be retrieved profile by profile. Notice that N_{0r}, N_{0s}, and N_{0g} are assumed to be constant for any individual vertical profile in all layers. This assumption would cause some uncertainty because in tropical cloud systems the wind shear could cause some vertical variation on PSD. However, the horizontal variation of the PSD is assumed to be much larger than its vertical variation and the use of different N_0 for rain, snow, and graupel can also overcome part of this problem.

The flowchart for the algorithm is shown in Fig. 1. Input fields for the radiative transfer model are built from various observation data sources. Initial hydrometeor content profiles are estimated from radar reflectivity Z measurements by using an N_0-scaled Z–M relationship derived from microphysical data fitting (Testud et al. 2001; GP). An iterative inversion is performed to retrieve the hydrometeor profiles by minimizing the difference between observed and calculated brightness temperatures.

a. The RTM

The original RTM used here was described by Kummerow and Weinman (1988). It is not our purpose to review in detail the principles of this RTM, but its main characteristics are described here. It is based on the one-dimensional Eddington approximation for a multilayered plane-parallel medium by solving the general microwave radiative transfer equation. The emissivity of the sea surface is calculated according to the incidence angle and polarization of the radiation, the sea surface temperature, the salinity, and the surface roughness induced by driven waves. For the atmospheric absorption, water vapor, molecular oxygen, and cloud water are taken into account. The Rayleigh approximation is used to compute the absorption coefficient of the cloud water. The Mie theory is employed to compute the absorption and scattering by precipitation-sized hydrometeors.

As given by Kummerow et al. (1996), the mean errors of this Eddington approximation relative to a Monte Carlo scheme model are generally small (about 2.7 K at 85 GHz and 1.2 K at 19 GHz). Thus, the brightness temperature calculation from the 1D Eddington approximation would cause uncertainties as small as 1–3 K for most tropical oceanic storms. These differences are of the same order as those obtained in the inversion procedure of this algorithm.

This RTM allows for six hydrometeor types (e.g., cloud ice, cloud liquid water, rainwater, snow, graupel, and hail). In this application to tropical cyclones and convection systems, only four hydrometeor types (e.g., cloud liquid water, rainwater, snow, and graupel) are considered. Cloud ice is not taken into account because of its negligible influence in most cases (Viltard et al. 1998), and updrafts are generally weak; therefore, hail is very rare in oceanic tropical convective systems (Zipser and LeMone 1980; LeMone and Zipser 1980; Jorgensen and LeMone 1989; Lucas et al. 1994; Zipser and Lutz 1994; Toracinta et al. 2002) and hurricanes (Jorgensen et al. 1985; Cecil et al. 2002). Densities are assumed as 1.0 g cm^{-3} for rain, 0.1 g cm^{-3} for snow, and 0.4 g cm^{-3} for graupel. This fixed-density assumption is ideal. The real density of graupel can range from 0.1 to 0.5 g cm^{-3} or even higher (Macklin 1962). In fact, a more reasonable retrieval could be made by using a density–diameter relationship for frozen particles instead of using a fixed-density assumption. However, it

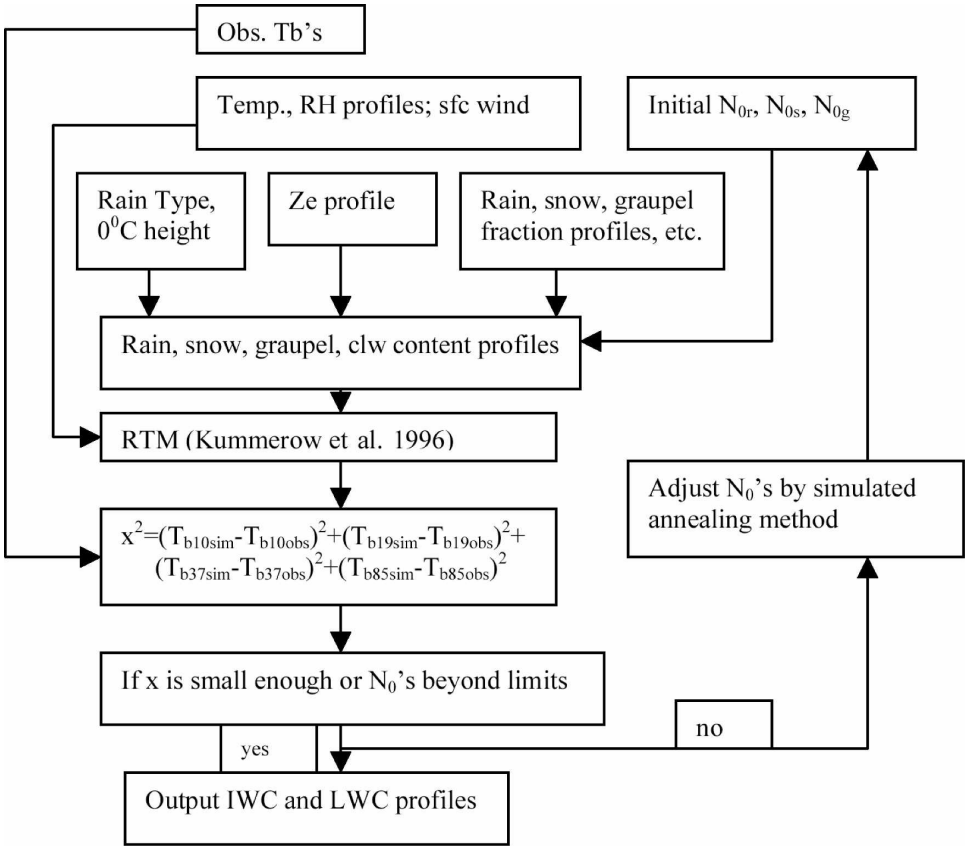

FIG. 1. The retrieval algorithm flowchart.

is hampered by the lack of a suitable density–diameter relationship from microphysics measurements.

In the RTM, flexibility exists in that the user can input the cloud profile and select the viewing angle, frequency, and polarization. It requires as input instrument specifications; the sea surface temperature; sea surface wind speed (WS); vertical profiles of temperature, height, and relative humidity; and PSDs of the hydrometeors in the cloud. In the RTM, the cloud liquid water distribution is assumed to be monodisperse. The distributions of rain, snow, and graupel are assumed to follow an exponential shape. All particles are assumed to be spherical in shape.

b. Hydrometeor content calculations

Joss and Gori (1978) noted that after accumulation over long intervals, the rain PSD is generally found to be close to exponential, but the "instant" PSD departs markedly from exponential. The gamma distribution has been introduced to account better for the shape of the distribution at the high rain rate observed by disdrometers. The gamma PSD is referred to as

$$N(D) = N_0 D^{\mu} e^{-\lambda D}, \tag{3}$$

where μ is the shape parameter of the gamma distribution. We see that when $\mu = 0$, a gamma PSD becomes an exponential PSD. A drawback of the gamma distribution is that the intercept parameter N_0 can no longer be considered a physical quantity, because its dimension itself ($m^{-4-\mu}$) is ill defined. Testud et al. (2001) developed a normalization approach to overcome this difficulty. They defined N_0^* as a normalized N_0 for the gamma PSD. Because N_0^* is equivalent to N_0 for an exponential PSD, it is physically meaningful. With this approach, any two integrated rainfall parameters (X, Y) can be expressed as

$$X = mN_0^{*(1-n)}Y^n, \tag{4}$$

where the coefficient n is dependent on μ, and m is dependent on μ and the particle density ρ. Both theoretical and observational evidence (Testud et al. 2001) indicates that m and n are only weakly dependent on μ; therefore, most precipitation-related relationships (e.g., radar reflectivity versus precipitation water content, radar reflectivity versus rain rate, reflectivity versus attenuation) strongly depend on N_0^* and only weakly depend on μ for a specific particle density. This property

has been exploited in many radar-only and radar–radiometer-combined profiling algorithms (Ferreira et al. 2001; Grecu and Anagnostou 2002; GP; Viltard et al. 2000), including the official TRMM precipitation radar (PR) 2A25 algorithm (Iguchi et al. 2000).

The μ-dependent m and n in (4) can be computed from fits to experimental data. In this study, for the rain region, we use an N_0^*-scaled Z–LWC relationship developed by M. Grecu [Goddard Earth Sciences and Technology Center (GEST), University of Maryland, Baltimore County (UMBC) and National Aeronautics and Space Administration (NASA) Goddard Space Flight Center (GSFC), 2004, personal communication] using polarimetric radar observations from Florida to obtain the rainwater content,

$$\mathrm{LWC} = 2.5 \times 10^{-6} N_0^{*0.412} Z^{0.588} \tag{5}$$

(LWC: g m^{-3}, N_0^*: m^{-4}, Z: mm^6 m^{-3}). This Z–LWC relation has coefficients very close to the one given by Viltard et al. (2000). This kind of relation is applicable for both exponential and gamma PSD. The cloud liquid water content is assumed to be 10% of the rainwater content, following the assumption of Tesmer and Wilheit (1998). The uncertainty caused by this assumption will be tested in the sensitivity test (section 3).

In the ice region, we develop an N_0^*-scaled Z–IWC relation by fitting 2D probe microphysics measurements during CAMEX-4 for temperatures below 253 K and apply it into all ice regions by assuming that this relationship is very weakly sensitive to the temperature (Viltard et al. 2000). The analysis of aircraft-sized distribution data is provided by Heymsfield, who uses an assumption of the density–diameter relationship derived by Heymsfield et al. (2002a) to calculate the IWC from the PSD measurements. We obtain the N_0^*-scaled Z–IWC relationship as follow:

$$\mathrm{IWC} = 2 \times 10^{-5} N_0^{*0.412} Z^{0.588}, \tag{6}$$

where N_0^* can be N_{0s}^* (for snow) or N_{0g}^* (for graupel). In (6), $m = 2.3 \times 10^{-5}$ represents the composite effect from all ice particles. Note that the coefficient m depends on the particle density also.

It is important to state assumptions and limitations of these procedures carefully. We must notice that (5) and (6) are obtained based on exponential or gamma PSD and specific tropical cloud microphysics observations. The assumptions used to derive them are similar to those used in many of the cited papers, but that is no assurance that they are correct. The exponents in (5) and (6) should contain significant uncertainties as the cloud system and scale vary. For example, Liu and Hallett (1998) proposed that from a system point of view, the maximum (minimum) likelihood cloud droplet size distribution is derived to be a Weibull (delta) distribution. They further argued that raindrop size distributions approach the exponential Marshall–Palmer distribution (Marshall and Palmer 1948) with increasing sampling sizes. The exponential PSD is essentially the limit when the sampling size approaches infinity. Therefore, our results may be compromised for small scales, that is, when the sampling period is less than 10 min (Liu and Hallett 1998).

Because we are concerned with both ice water and rainwater, a parameterization of the snow and graupel fraction profile is needed to simulate brightness temperatures at 37 and 85 GHz. From microphysical measurements in field programs, Stith et al. (2002) found that stratiform precipitation above the melting layer has no graupel in significant amounts, so we assume there to be all snow. In the convective rain region, the amount of graupel varies from case to case, so we refer to the hurricane modeling results by Lord et al. (1984, see their Fig. 6) and assume that graupel distribution reaches its maximum at 6 km, and snow distribution reaches its maximum at 12 km. We keep the vertical shape of snow/graupel water content the same as the results in Fig. 6 of Lord et al. (1984), but the specific value of the snow fraction (f_s) is controlled based on 85-GHz brightness temperatures (see section 3 for details). A sensitivity test for the snow/graupel fraction will be performed in section 3.

One-hundred-percent liquid water is assumed below the bottom of the melting layer for all rain types. The melting layer is defined as a layer around the 0°C level. The layer thickness is 1000 (1500) m for the stratiform (convective/intermediate) rain region. This is similar to the melting layer definition used in the TRMM 2A25 algorithm (Iguchi et al. 2000). A linear interpolation is used to set the fraction of rain, snow, and graupel within the melting layer for all rain types. The freezing level is found based on the radar brightband height for CAMEX-4 data. A mass flux continuity assumption is used in the liquid–ice transition layer.

c. Inversion procedure

We iteratively look for the set of N_0^*s that leads the RTM to calculate simulated brightness temperatures that are as close as possible to the observed ones. The inversion is done iteratively from the initial values. At each iteration, the error function is defined by the sum of the square of the errors in four channels at 10, 19, 37, and 85 GHz,

$$\chi^2 = \sum_{i=1}^{N_f} q_i (T_{b\mathrm{sim}i} - T_{b\mathrm{obs}i})^2, \tag{7}$$

where N_f is the number of independent frequencies used in this retrieval, which corresponds to the number of independent brightness temperatures to be adjusted. Here $T_{b\mathrm{sim}i}$ and $T_{b\mathrm{obs}i}$ are, respectively, the calculated and observed brightness temperatures for the ith frequency. In application to CAMEX-4 data, T_b represents the nadir-viewing brightness temperature without polarization effect. The coefficient q_i is a weighting factor that allows us to control the contribution from a given frequency. In fact, a covariance matrix-based cost function and weighting factor could make the error analysis process more physical, but it requires more detailed information on surface conditions (e.g., temperature, wind speed, and sea foam fraction) and hydrometeor states (e.g., sizes, shapes, and densities).

This inversion is performed by searching for the minimum of the error function numerically. The simulated annealing technique (Goffe et al. 1994) is used in this inversion. The features of this technique are that 1) it explores the function's entire surface and tries to optimize the function while moving both uphill and downhill, 2) it is largely independent of the initial values and step lengths, and 3) it can escape from local optima and go on to find the global optimum. Its code is flexible to allow users to set the upper and lower limits of the iteration parameters. For N_0^* unknowns in our problem, we set the lower bound LB = 10^4 m^{-4}, and upper bound UB = 10^9 m^{-4}. Other parameters in the simulated annealing method, such as temperature T and the temperature reduction factor RT, are useful in the adjustment of the running speed, but the algorithm convergence is not sensitive to the choice of T and RT as long as $T > 5.0$ and RT > 0.85. The sole drawback to simulated annealing is the required computational power. Currently, on a common 1.5-GHz single central processing unit (CPU) Linux-based personal computer, it takes about 5 min to obtain one retrieved profile.

As pointed out by Viltard et al. (1998), this inversion must be overdetermined because of the noise in the measurements and possible ambiguity of the solution. Thus, the four independent brightness temperatures only allow us to retrieve three variables, which are N_0s for rain, snow, and graupel in this algorithm.

3. Sensitivity tests

To understand the effects of the input parameters on the microwave radiation and to predict the error for our retrievals, we simulated the AMPR nadir T_b uncertainties associated with the sea surface wind speed, vertical profiles of the temperature and relative humidity, cloud ice, cloud liquid water below the freezing level, the snow–graupel fraction in ice regions, and the supercooled liquid water above the freezing level. Those retrieval inputs, along with the instrument noise, are the major error sources. Although a lack of the melting layer representation in the RTM could also cause some uncertainties (Nesbitt et al. 2004), the effect of melting particles is currently not considered in this algorithm because it is uncertain how to simulate the bright band. Although some idealized simulation studies on this issue have been done by Olson et al. (2001a,b), many uncertainties exist when applied to real data.

Our final retrievals are LWC and IWC profiles. However, here we test the sensitivities by using only the integral values LWP and IWP because the vertical distribution (or shape) of LWC and IWC is determined by the radar reflectivity profile in this algorithm. To provide sensitivity tests of individual error sources, all parameters (e.g., surface wind speed and the profile of temperature and relative humidity), except the one to be tested, that are used in the RTM are fixed at the mean values of observations in tropical cyclones during CAMEX-4. The brightness temperature errors are then determined from an uncertainty in the tested parameters. For the snow fraction (f_s; therefore the graupel fraction is $1 - f_s$), because there are no reference values, a series of f_s from 100% to 0% will be tested. In this sensitivity test, the Marshall and Palmer (1948, hereinafter MP) PSD distribution is assumed for rain and snow, and the Rutledge and Hobbs (1984, hereinafter RH) PSD is assumed for graupel. This strategy is similar to the one used in Prasad et al. (1995), in which the MP distribution is used for rain and for ice at upper levels of the cloud (above 6 km) and the RH scheme for ice at lower layers of the cloud (below 6 km). In the RH PSD, N_0 is 0.04 cm^{-4} to represent a flatter slope resulting from much larger particles. Input hydrometeor profiles to the simulation are selected from the Earth Resources (ER)-2 Doppler radar (EDOP)-derived profiles of observations of tropical oceanic precipitation systems with both the rain and ice layers (i.e., not warm rain profiles) during CAMEX-4. Because in the selected profiles, a small (large) LWP corresponds to a small (large) IWP, the following figures only show either LWP or IWP as the x-axis parameter.

Before looking at the results of the sensitivity tests, we need to estimate how much uncertainty could be caused by the RTM and the instrument errors. As mentioned in section 2a, the accuracy of the RTM-calculated T_b is estimated at about 1–3 K, depending on the atmospheric situation, and accuracy of the different channels of the radiometers is estimated at about 3–5 K. Therefore, the total uncertainty is about 4–8 K.

First, the absolute value of the T_b error (DT_b) caused by an error of ± 5 m s^{-1} in the surface WS is calculated.

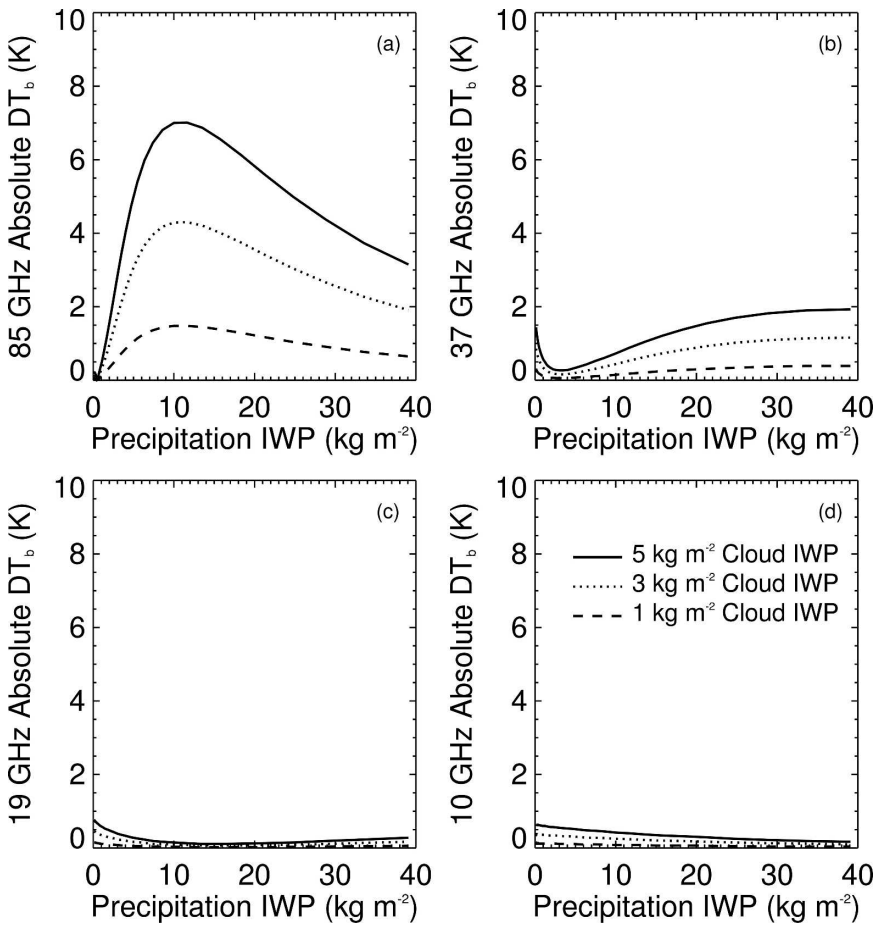

FIG. 2. Simulated absolute values of uncertainties of (a) 85-, (b) 37-, (c) 19-, and (d) 10-GHz nadir brightness temperatures (DT$_b$s) resulting from the existence of 1, 3, 5 kg m^{-2} cloud IWP.

Uncertainties of T_bs to wind speed decrease exponentially with the intensity of the precipitation. As the LWP value reaches 3 kg m^{-2} (or 3 mm), all DT$_b$s are below 3 K, which is within the RTM Eddington approximation error. It is also noticed that the uncertainties at high frequencies (85 and 37 GHz) caused by this wind error are usually very small for LWP greater than 1 kg m^{-2} and can be neglected. The wind speed-related error is significant only for no-rain regions with large wind variability, such as the interior of the eye, which is not a focus of this paper.

The test results on the effect of the ±2 K error in the temperature profile (including sea surface temperature) show that the 85-GHz T_b uncertainty is about 3–4 K, which is within the RTM Eddington approximation error. The T_b uncertainties caused by the relative humidity error have the similar behavior as those caused by temperature error, but they are much smaller. In precipitation clouds (LWP greater than 1 kg m^{-2}), a ±10% error of the relative humidity is typical. For this much error, the T_b uncertainty for 10, 19, and 37 GHz is much less than 1 K, and at 85 GHz is around 1 K.

In the algorithm, we neglect the effect from the cloud ice. To determine the uncertainty caused by this assumption, Fig. 2 presents the absolute value of the T_b error caused by the existence of 1, 3, 5 kg m^{-2} cloud IWP at 10, 19, 37, and 85 GHz, respectively. By examining the 2A12 output for the 1-yr TRMM tropical cyclone data (Jiang 2004), we estimate that the maximum and mean cloud IWP values for tropical cyclones are 5 and 0.4 kg m^{-2}. From Fig. 2, we see that the largest uncertainty caused by the cloud ice is at 85 GHz. For a 5 kg m^{-2} cloud IWP, the absolute 85-GHz DT$_b$ could reach 7 K at the precipitation IWP value of 10 kg m^{-2}, which is still within the total uncertainty of RTM and instrument errors.

In the retrieval, the cloud liquid water is assumed to be 10% of the rainwater in the tropical oceanic precipitation system. This will cause some uncertainty because the extinction coefficient is proportional to the liquid

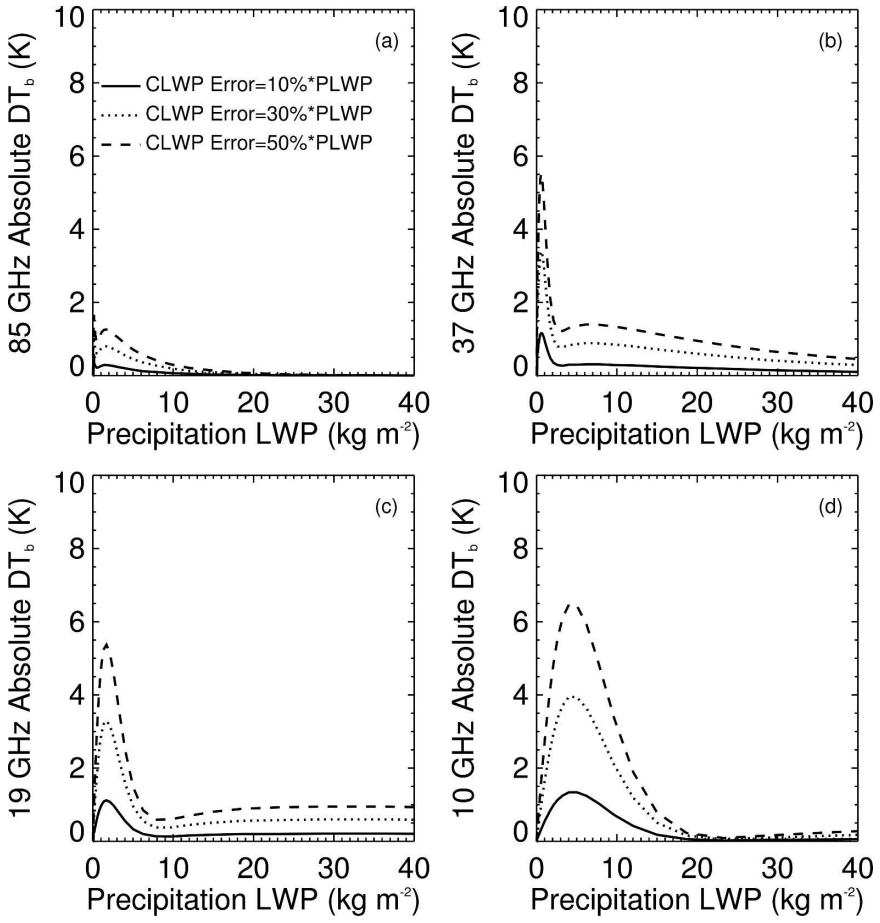

FIG. 3. Simulated absolute values of uncertainties of (a) 85- (3.5 mm), (b) 37- (8.1 mm), (c) 19- (15.8 mm), and (d) 10- (30.0 mm) GHz nadir brightness temperatures (DT_bs) resulting from the cloud LWP errors of 10%–50% of precipitation LWP.

water mass for sufficiently small particles at the microwave band, and the amount of the cloud liquid water varies case by case; it could be as low as only 5% or as high as 20% of the rainwater content as shown in the 2A12 output for a 1-yr TRMM tropical cyclone database (Jiang 2004). Figure 3 shows the absolute value of DT_b caused by the cloud LWP errors of 10%–50% of precipitation LWP at 10, 19, 37, and 85 GHz, respectively. In the cloud liquid water sensitivity test, the cloud liquid water is present mainly below the freezing level. The effect of the supercooled liquid water will be examined later. From Fig. 3, we see that the largest uncertainty is at 10 GHz, and it is less than 8 K.

In simulating the effect of the variation of the snow–graupel fraction, we keep graupel in the lower (maximum at 6 km) and snow in the upper (maximum at 12 km) layers, but change the total fraction of snow in this sensitivity test. It is found that the variation of f_s has no significant effect on T_bs at 10 and 19 GHz, so we examine this effect only for higher frequencies based on IWP. In addition to 37 and 85 GHz, which are the channels we use for the retrieval, the T_bs at 50 and 52 GHz are also investigated because we want to use the independent observations in these channels to validate our retrieval indirectly. Because these channels are around the oxygen emission lines and were originally designed for measuring the temperature sounding (Lambrigtsen and Riley 2002), it is necessary to determine if they are sensitive to rain emission or ice scattering. If not, then this kind of validation would be not meaningful.

Figure 4 shows the T_bs at 85, 52, 50, and 37 GHz as a function of IWP for the snow fraction at 100%, 90%, 75%, 50%, 25%, 10%, and 0%, with a $f_s = 100\%$ representing pure stratiform rain regions. Variability of the T_b depressions with the snow–graupel fractions is evident, with the 85-GHz channel representing the largest change. Similar relations were found by Vivekanandan et al. (1991), in which the 85-GHz T_b is a different function of the 85-GHz optical thickness for different bulk ice densities from 0.2 to 0.9 g cm^{-3} for a simulation

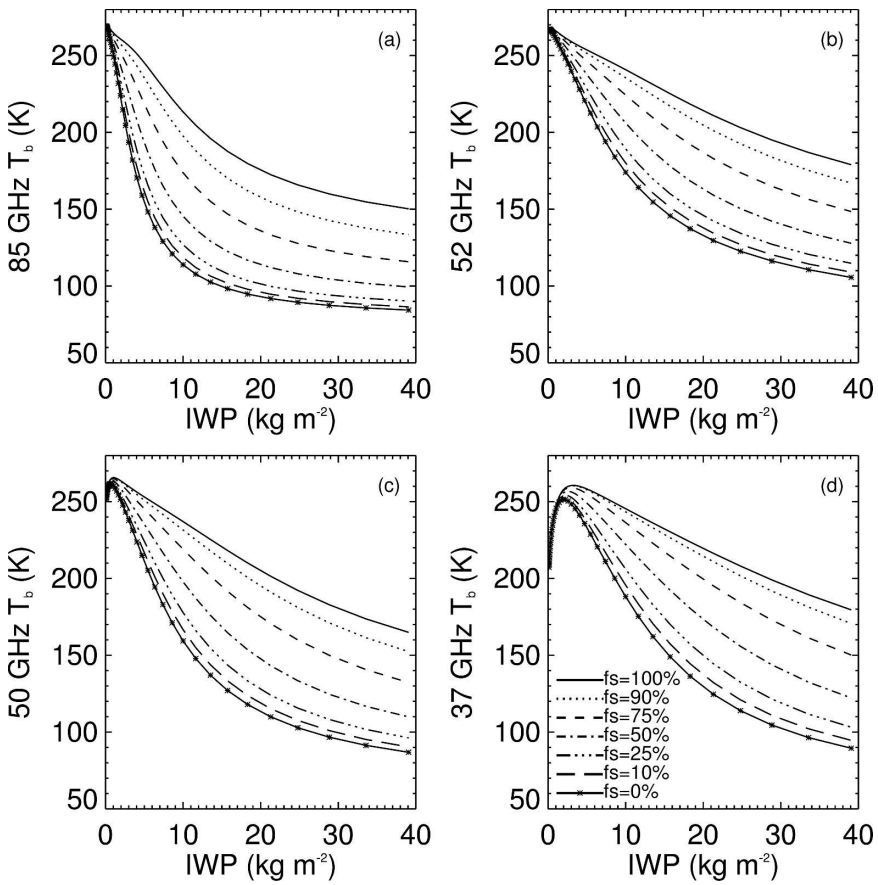

FIG. 4. Simulated nadir view brightness temperatures at (a) 85 (3.5 mm), (b) 52 (5.8 mm), (c) 50 (6.0 mm), and (d) 37 GHz (8.1 mm) as a function of IWP for snow fractions of 100%, 90%, 75%, 50%, 25%, 10%, and 0%.

of a continental hail storm. In their model, only one frozen hydrometeor was assumed, so the bulk ice density effect there is similar to the snow–graupel fraction effect in our simulation here. Notice that the equivalent bulk ice densities in this study range only from 0.1 to 0.4 g cm^{-3}, neglecting some high-density ice particles in tropical oceanic storms. Again, it is not impossible that high-density ice particles could exist in these kinds of storms.

It is pretty clear that the snow–graupel fraction represents the dominant error source in this retrieval. In stratiform regions, this effect is minimized because observational studies have shown that graupel is not present in tropical oceanic precipitations in significant amounts (Stith et al. 2002; Black and Hallett 1986, 1999). However, in convective regions, graupel may be present, but its relative amount is uncertain. A convective intensity–dependent snow–graupel fraction scheme is needed to decrease this uncertainty. Fiorino (2002) examined the microphysics data during the Kwajalein Experiment (KWAJEX) and concluded that, on average, graupel contributes from about 70% at 4–5 km to 20% at 9–10 km of the total ice water content. This result corresponds to an about 50% graupel fraction on average. In this study, we use 85-GHz T_b as the indicator of the convective intensity. As mentioned in section 2b, hurricane-modeling results from Lord et al. (1984) are used to assume the vertical shape of the snow–graupel water content. In the meantime, we also use the 85-GHz T_b as a convective intensity indicator to control the vertically integrated snow–graupel fraction. For 85-GHz T_b less than 200 K, f_s = 25% is assumed; for 85-GHz T_b greater than 200 K but less than 230 K, f_s = 50% is assumed; for 85-GHz T_b greater than 230 K, f_s = 75% is assumed. Here f_s refers to the integral snow fraction corresponding to the total IWP. We keep the vertical distribution of snow maximized at 12 km and of graupel at 6 km as mentioned in previous section. The above-85-GHz T_b thresholds were estimated from examples of AMPR–EDOP observations. They are somewhat arbitrary.

From Figs. 4b and 4c, in convective situations, the T_b

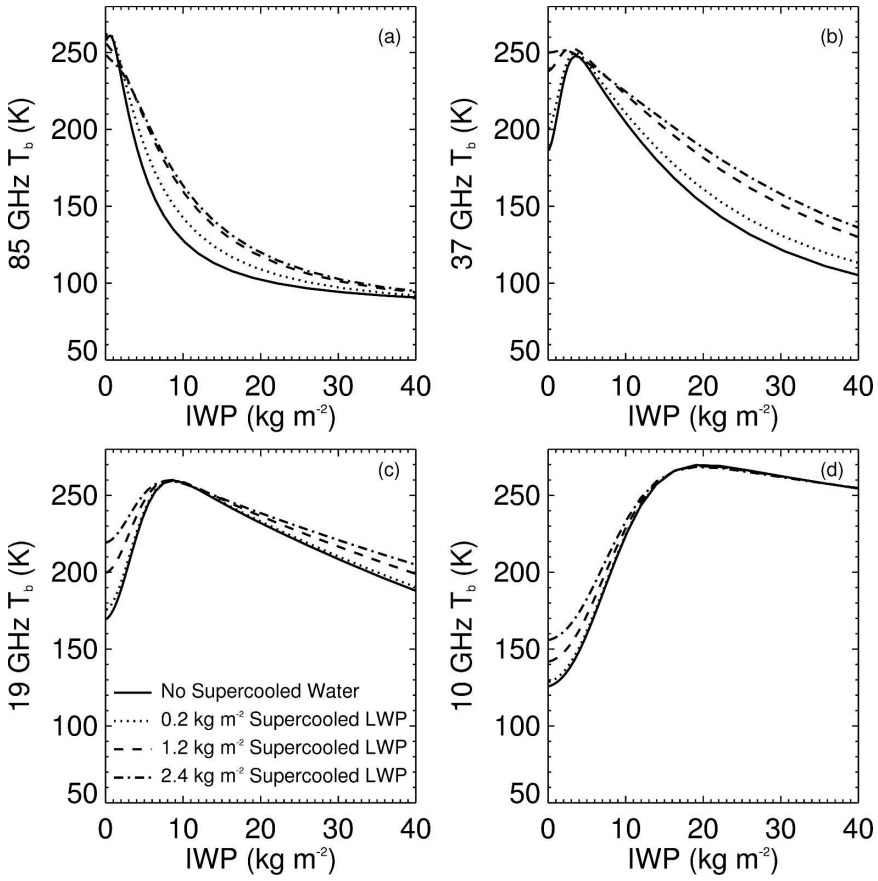

FIG. 5. Simulated nadir view brightness temperatures at (a) 85, (b) 37, (c) 19, and (d) 10 GHz as a function of IWP for supercooled LWPs of 0, 0.2, 1.2, and 2.4 kg m^{-2}.

depression at 52 and 50 GHz could reach 60 and 65 K, respectively, for IWP = 10 kg m^{-2} and f_s = 50%. The corresponding values for 85 and 37 GHz are 120 and 40 K, respectively. It can thus be concluded that the radiative transfer characteristics of 50 and 52 GHz are in between those of 85 and 37 GHz and could be a good indicator for ice scattering in convective situations. However, it is noticed that the T_b depression at 52 GHz is less than that for 50 GHz. This is a sign that shows that the 52-GHz radiation is contaminated by the oxygen emission line at about 54 GHz. Although we could use the 52-GHz channel to identify ice scattering in convective regions, we should use it with caution in stratiform regions because, in these situations, the T_b depressions are not very large and are easily contaminated by oxygen emission. For the 50-GHz channel, the oxygen emission contamination is minimized and this channel could be used as an independent validation source.

The combined algorithm assumes no supercooled rainwater above the freezing level. This may be true for most cases because the strength of updrafts in tropical cyclones is generally very weak (Jorgensen et al. 1985; Cecil et al. 2002). However, for some extreme cases, "hot towers" might exist in hurricanes (Simpson 1963; Black et al. 1994; Herman and Heymsfield 2003; Black et al. 2003; Heymsfield et al. 2001). The strong updraft in this region could bring some liquid water aloft. In the ice region, in addition to snow and graupel species, there could be a certain amount of supercooled water. Even in modest updraft regions, supercooled cloud and rainwater in the summertime in Florida could be up to a few grams per cubic meter (Hallett et al. 1978; Keller and Sax 1981). Figure 5 shows the effect of the existence of 0.2, 1.2, and 2.4 kg m^{-2} supercooled LWP between 6 and 10 km. We see that the increase of T_bs at four channels resulting from the existence of the supercooled water is evident. For example, at 85 and 37 GHz, the T_b increases are up to 40 K resulting from 2.4 kg m^{-2} of supercooled LWP. Therefore, the no-supercooled-water assumption in the combined algorithm could cause some uncertainty for both ice and liquid water amounts. Specifically, if a strong convective core contained large supercooled liquid water, the

TABLE 1. Characteristics of the seven CAMEX-4 flight legs [here yy indicates last two digits of the year (20yy), mm is month, and dd is day].

	Flight date (yymmdd)	Time (UTC)	Storm	DC-8 altitude (km)	Total sample	Stratiform sample	Convective sample	No-rain sample
EDOP–AMPR–PMS dataset	010922	1932–1940	Humberto	8.5	104	72	32	0
	010923	2033–2053	Humberto	10.6	240	188	52	0
	010924	2128–2142	Humberto	11.2	170	145	25	0
	010909	1833–1842	MCS	8.9	113	88	25	0
EDOP–AMPR–HAMSR dataset	010910	1650–1715	Erin	—	301	257	20	24
	010910	1754–1822	Erin	—	325	157	70	98
	010910	1914–1947	Erin	—	393	313	17	63
Total number of samples					1646	1220	241	185

ice water content of that core would be significantly underestimated.

4. Application to CAMEX-4 observations

a. Dataset

Observations from CAMEX-4 (Kakar et al. 2006) are used in the retrieval algorithm. This work focuses on the data from three instruments on the ER-2 aircraft and one instrument on the DC-8 aircraft. Onboard the ER-2, flying at a 20-km altitude, the instruments of interest are the EDOP (Heymsfield et al. 1996), AMPR (Spencer et al. 1994), and High Altitude Monolithic Microwave Integrated Circuit (MMIC) Sounding Radiometer (HAMSR; Lambrigtsen and Riley 2002). The EDOP is an X-band (9.6 GHz) radar with a high spatial resolution. The AMPR is a passive radiometer observing at 10.7, 19.35, 37.1, and 85.5 GHz. The HAMSR, used only for validation purposes, is a passive microwave radiometer with eight channels near the oxygen absorption lines at 50–56 GHz and seven channels near 183.31 GHz. The HAMSR channels are independent of any channels used in the retrieval. On the DC-8 aircraft, flying at about 11-km altitude, the cloud microphysics data from Particle Measuring Systems, Inc., (PMS) 2D cloud (2D-C) and 2D precipitation (2D-P) probes are used as a comparison data source. The 2D-C and 2D-P probes measured PSDs from about 100 μm to 6 mm in various increments (Heymsfield et al. 2006).

A collocated dataset is obtained from seven flight legs on 9, 10, 22, 23, and 24 September 2001. Three of them are from Hurricane Erin (10 September), two are from Hurricane Humberto (23, 24 September), one is from Tropical Storm Humberto (22 September), and one is from a Gulf of Mexico mesoscale convective system (MCS; 9 September). A dominant part of this dataset is from tropical cyclones. To facilitate collocation of passive and active microwave measurements from the AMPR and EDOP, only the nadir view data from these instruments are considered. At nadir, the AMPR measurements represent an equal mix of horizontal and vertical polarization. When matching EDOP and AMPR data, a 1-km horizontal grid is chosen, which is close to the EDOP surface footprint (1.1 km). EDOP and AMPR data are averaged/interpolated into the 1-km grid points. The rain type is classified subjectively, using the EDOP reflectivity and Doppler velocity observations. A Gaussian fit to the vertical reflectivity profile (G. Heymsfield and L. Belcher 2001, personal communication) is used to identify the brightband height in stratiform regions, therefore determining the freezing level. For convective regions, the freezing levels determined from neighboring stratiform regions are used and interpolated. EDOP suffers from the attenuation problem, especially in intensive convective precipitation. The EDOP attenuation correction is performed by using the surface reference technique (Tian et al. 2002).

For the seven flights, a total of 1646 collocated samples are found, of which 1019 samples are from the three Erin flights with HAMSR observations available (therefore, the EDOP–AMPR–HAMSR dataset); the remaining 627 samples are from the 9, 22, 23, and 24 September flights with the DC-8 aircraft in situ PMS 2D-C and 2D-P microphysics data available at about 9–11-km altitude (therefore, the EDOP–AMPR–PMS dataset). Table 1 shows a summary of these seven flight leg datasets. The parameters derived from in situ measurements are averaged into a 1-km grid to be matched with EDOP–AMPR data. For comparison with the retrieval, the LWC and IWC profiles are also calculated by applying empirical Z–M relations to EDOP reflectivity measurements, in which the Z–IWC relationship is from Black (1990) and the Z–LWC relationship is from Willis and Jorgensen (1981) (therefore, the radar-only or Z–M algorithm). Coincidentally, the Black (1990) Z–IWC relationship happens to be very close to our initial Z–M–N_0 relationship in (6) if $N_0 = 1.4 \times 10^6$ m^{-4}. A simplified version of the GP algorithm is used for comparison purposes; it is the same as the current algorithm, except for assuming only one N_0 as being unknown for rain, snow, and graupel.

TABLE 2. Statistical results for the differences between retrieved and observed T_bs. Here DT_b stands for $T_{b\text{retrieved}} - T_{b\text{observed}}$ and σDT_b stands for standard deviation of the above-mentioned difference.

Total number of samples (1646)	No rain (185 samples)	Stratiform (1220 samples)	Convective (241 samples)
Mean DT_{b10}	−10.09	−0.40	−1.57
Mean DT_{b19}	−10.82	1.66	−1.68
Mean DT_{b37}	−12.15	−4.03	−5.28
Mean DT_{b85}	−5.44	2.64	−0.18
σDT_{b10}	11.29	5.53	7.25
σDT_{b19}	12.66	5.65	7.70
σDT_{b37}	15.55	6.61	8.04
σDT_{b85}	5.71	3.81	4.49

b. Quality of inversion

Numerous tests of the simulated annealing inversion procedure tend to demonstrate the stability of the method and its independence of initial values. As mentioned in section 3, the total uncertainty from the RTM and instrument errors is about 4–8 K.

The statistical difference between the retrieved and observed T_bs (DT_bs) obtained from the total retrieval of 1646 data points are presented in Table 2. The magnitude and sign of the differences depends upon the frequency and the observed situation (e.g., stratiform, convective, or no rain). Because there is theoretically no interaction with water particles, it may be considered roughly that the no-rain situation represents an estimation of the error of instrument calibration, sea surface, and atmospheric characteristics (sea surface wind speed, vertical profiles of temperature, and relative humidity). In this dataset, no-rain samples are mostly from the eye region of Hurricane Erin. Because of the large variation of sea surface wind speed in eye regions and the large sensitivity of the simulated brightness temperatures at low frequencies to the wind speed, as discussed in section 3, it is not surprising that the absolute mean and standard deviation of the differences are around 10–15 K at 10, 19, and 37 GHz. In addition, the no-rain situations in this study are not precisely identifiable and thus can be cloudy or slightly precipitating, which adds more uncertainties.

All DT_bs in stratiform and convective regions are below 7–8 K, within the total uncertainty of RTM and instrument errors. The absolute mean values and standard deviations of DT_bs in convective situations are mostly larger than those for stratiform situations, showing that there are more variations of microphysics characteristics in convective conditions and it is thus harder to simulate. Among these frequencies, the 37-GHz T_b is influenced by both rain emission and ice scattering, so it is highly sensitive to simulation errors. The melting layer crudely taken into account in this simulation may lead to a systematic error. However, the T_bs at 10 and 85 GHz are the ones that correspond to the best fit, whatever the considered situations. This result is probably because of the fact that the 10-GHz channel is only sensitive to the rain emission and the 85-GHz frequency is essentially sensitive only to the ice precipitation, and therefore they are easy to adjust.

c. Comparisons of IWC retrievals with aircraft in situ measurements and simplified GP and radar-only estimates

Several factors make it difficult to make comparisons of remotely obtained precipitation microphysical parameters with direct in situ measurements from aircraft. First, the sample volumes are vastly different. At a normal DC-8 aircraft speed of about 210 m s^{-1}, the 2D-C and 2D-P probes sample the air at the rate of 0.007 $m^3 s^{-1}$ and 1 $m^3 s^{-1}$, respectively (Heymsfield et al. 2006). Therefore, it takes about 2.5 min to sample 1 m^3 air. For EDOP, the sample volume for each pulse at 11-km altitude (the normal DC-8 flight height during CAMEX-4) is about 2×10^6 m^3. AMPR samples the whole layer of the precipitation in its beamwidth, so the sample volume is much larger than that for EDOP. Second, the sampling period for the aircraft microphysics instruments has to be long enough to obtain a number of particles in each bin to make sense in obtaining the drop size distribution. Third, it is very difficult to get exactly matched ER-2 and DC-8 flight tracks for both distance and time. We carefully choose EDOP and DC-8 flight tracks that match each other closely in distance (mostly within 1–2 km for the 627 collocated samples), but have time differences of up to 4 min. The inhomogeneous nature and the time evolution of the precipitating clouds, especially in convective cores, makes the different sample volumes a serious problem for intercomparison purposes. The fourth difficulty arises from the large variation of ice particle densities, which makes the estimation of bulk parameters, such as IWC, from the size distribution measurements subject to uncertainties. In this study, the analysis of aircraft-sized distribution data is provided by Heymsfield, who uses an assumption of density–diameter relationship derived by Heymsfield et al. (2002a) to calculate the IWC. The uncertainty of this IWC estimate is about 25%, as given by Heymsfield et al. (2002b). However, the actual uncertainty of this estimate might be even higher because of the ice density uncertainty (Korolev et al. 2004).

Despite the uncertainties in aircraft measurements and difficulties inherent in sampling the same cloud volume with 2D probes and aircraft remote sensors,

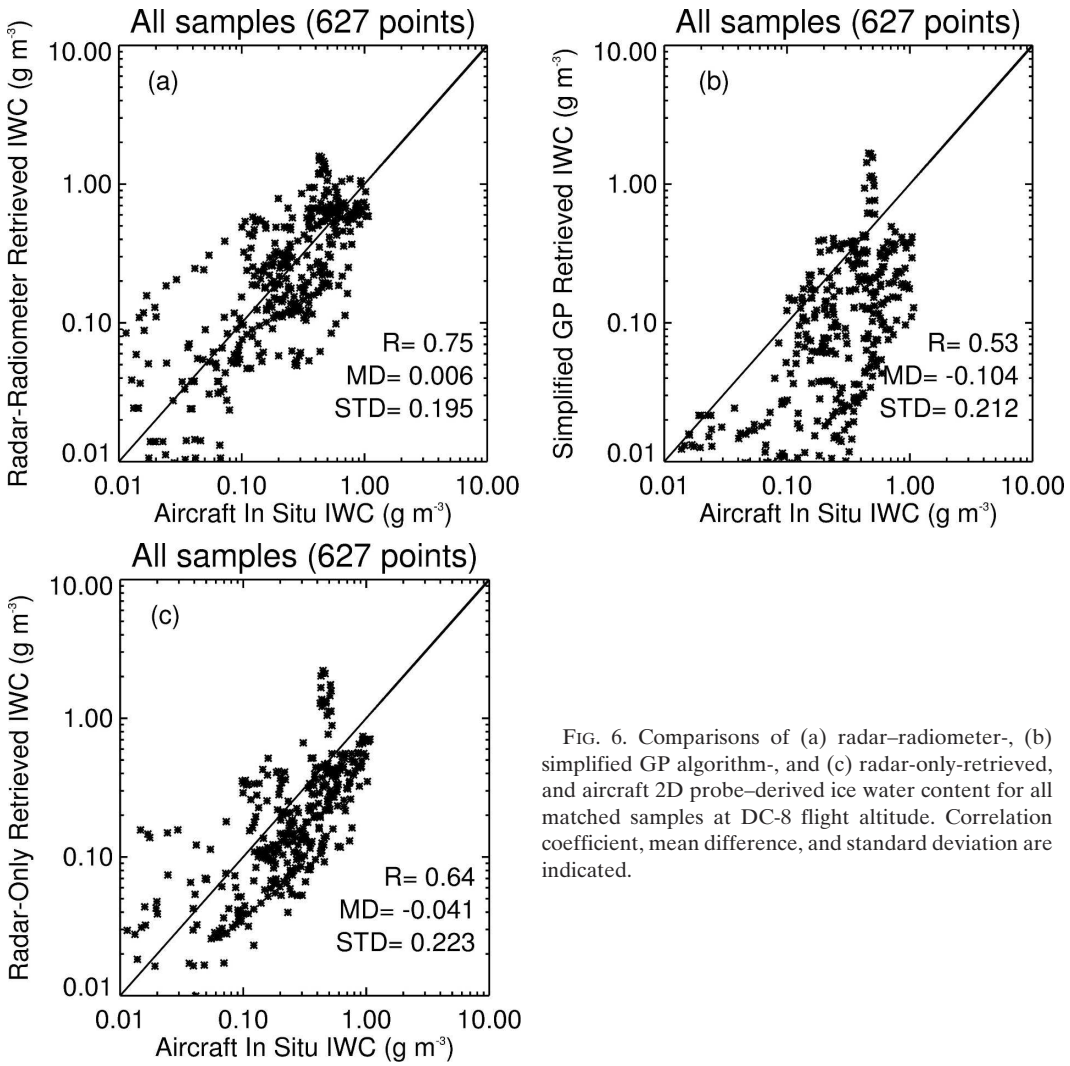

FIG. 6. Comparisons of (a) radar–radiometer-, (b) simplified GP algorithm-, and (c) radar-only-retrieved, and aircraft 2D probe–derived ice water content for all matched samples at DC-8 flight altitude. Correlation coefficient, mean difference, and standard deviation are indicated.

comparisons between retrieved results with in situ measurements are widely used to judge the performance of algorithms (Mace et al. 1998; Wang and Sassen 2002; Skofronick-Jackson et al. 2003). However, an awareness of the limitations helps us to better understand the differences in the results from aircraft and remote sensing measurements. The traditional point-to-point comparison is based on the assumption that they have sampled the same cloud volume. The statistical comparisons have the advantage that minimizes the sample volume issues. Therefore, only the latter approaches will be used.

Figure 6 shows the scatterplot of radar–radiometer-, simplified GP-, and radar-only-estimated IWC versus 2D probe-derived IWC at DC-8 flight altitudes from 8.5 to 11 km for the 627 samples in the EDOP–AMPR–PMS dataset. From Fig. 6a, the mean difference (MD) of the retrieved and 2D-derived IWC is very small, only 0.006 g m^{-3}, and the standard deviation (STD) is 0.195 g m^{-3}. However, the correlation coefficient (R) is only 0.75; a lot of scatter might be because of the mismatch of the two airplanes and the very different sample volumes.

For comparison, Fig. 6b (Fig. 6c) is like Fig. 6a except that the y axis shows the IWC derived by the simplified GP algorithm (radar-only Z–M method). It is apparent that the simplified GP algorithm (radar-only method), with an MD of -0.104 (-0.041) g m^{-3}, systematically underestimates the IWC when compared with 2D probe measurements and the combined radar–radiometer retrievals. The simplified GP estimates are even worse than radar-only estimates for IWC. This is mainly because of the unreasonable microphysics assumption of GP, for example, the same N_0 for rain, snow, and graupel. Although it is considered the classical Z–IWC relation in hurricanes, Black's (1990) regression was obtained from very limited aircraft datasets at a flight altitude of about 6 km; it cannot

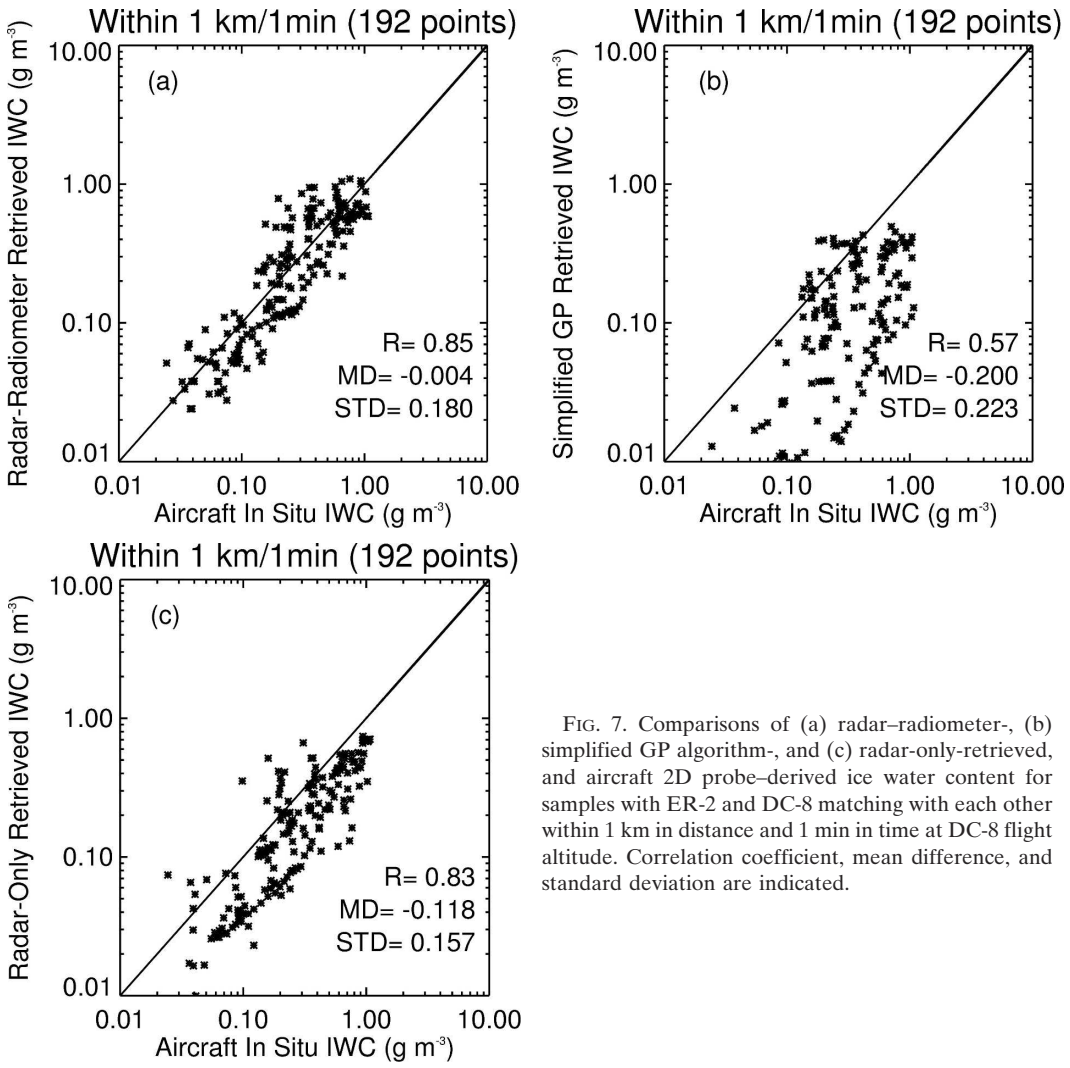

FIG. 7. Comparisons of (a) radar–radiometer-, (b) simplified GP algorithm-, and (c) radar-only-retrieved, and aircraft 2D probe–derived ice water content for samples with ER-2 and DC-8 matching with each other within 1 km in distance and 1 min in time at DC-8 flight altitude. Correlation coefficient, mean difference, and standard deviation are indicated.

represent all of the situations in nature. However, the EDOP in the 32.0-mm wavelength has a tendency of missing some of small ice particles that could be detected by the AMPR high-frequency channels (85 GHz equivalent to 3.52-mm wavelength). The combined radar–radiometer algorithm adjusts the PSD for each profile to obtain a best agreement with radiometer observations; this kind of physical adjustment represents a promising improvement over radar-only empirical retrievals.

To check the effect of mismatch on the comparisons, Fig. 7 shows the same comparisons as in Fig. 6, but only for the samples in which ER-2 and DC-8 match each other within 1 km in distance and 1 min in time. The comparison is clearly less scattered. From Fig. 7a, a higher correlation coefficient (0.85) and lower MD (-0.004 g m^{-3}) and STD (0.18 g m^{-3}) are also obtained, which confirms the importance of spatial and temporal variability. From Fig. 7b (Fig. 7c), however, the underestimate of the simplified GP algorithm (radar-only method) is more severe for these 192 within 1 km–1 min samples.

Considering the uncertainties in calculating IWC from in situ samples and the limitations of the comparison discussed above, we can conclude from Fig. 6a and Fig. 7a that the agreement between radar–radiometer-retrieved and aircraft-measured IWC is as good as can be expected.

Now let us examine the retrieval performance for different rain types. Figure 8 shows the scatter comparison between retrieved and 2D probe–measured IWC for stratiform situations for both the 493 samples from the original 627 total samples and the 137 samples from the total 192 within 1 km–1 min samples. The correlation coefficients are 0.9 and 0.92, the MDs are 0.007 and 0.005 g m^{-3}, and the STDs are 0.125 and 0.087 g m^{-3},

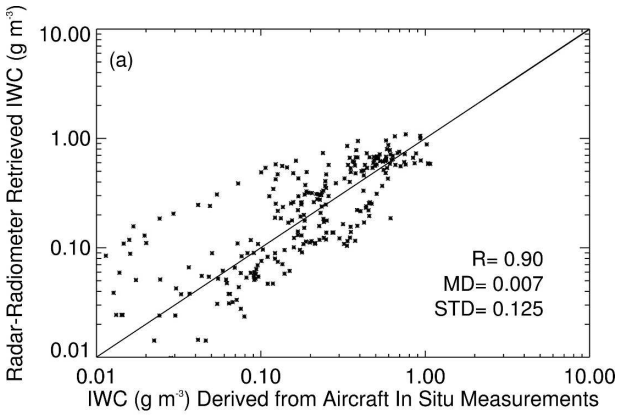

FIG. 8. Comparisons of radar–radiometer-retrieved and 2D probe–derived ice water content at DC-8 flight altitude for (a) all stratiform samples and (b) ER-2 and DC-8 matching within 1-km–1-min stratiform samples. Correlation coefficient, mean difference, and standard deviation are indicated.

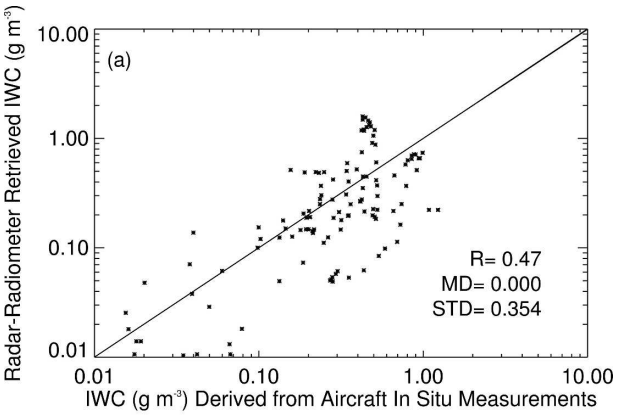

FIG. 9. Comparisons of radar–radiometer-retrieved and 2D probe–derived ice water content at DC-8 flight altitude for (a) all convective samples and (b) ER-2 and DC-8 matching within 1-km–1-min convective samples. Correlation coefficient, mean difference, and standard deviation are indicated.

respectively. Even in stratiform regions, the inhomogeneous nature is obvious because the comparison in Fig. 8a is more scattered than that in Fig. 8b; the standard deviation is larger too. However, the higher correlations and lower standard deviations for the total samples shown in Figs. 6a and 7a mean that the radar–radiometer retrieval has a better performance in stratiform situations.

The comparisons between retrieved and 2D probe-derived IWC for convective situations for both the original samples and the within1 km–1 min samples are shown in Fig. 9. In general, there is a lot of scatter in convective regions. There is less scatter for the samples within 1 km–1 min, but the improvement is small. The correlation coefficients are only 0.47 and 0.66, respectively, while the standard deviations are high (up to 0.354 and 0.193 g m^{-3}). Considering the nature of life cycle and dimension characteristics of convective cells (only several minutes and several kilometers), this result is not surprising. The different sample volume issue is maximized in this condition. At the same time, the snow–graupel fraction assumption in our algorithm also contributes some uncertainties in convective regions.

By comparing with aircraft in situ observations, it is clear that the combined radar–radiometer algorithm has a quite good performance in stratiform situations. In convective precipitation, although there is no systematic under- or overestimation, the retrievals tend to have large variations around in situ measurements. This can partly be explained by the mismatch and different sample volume issues in these comparisons, but the main reason is the assumptions in the algorithm.

d. Comparisons of 50-GHz brightness temperature calculations with HAMSR observations

The sensitivity test in section 3 using RTM simulations has shown that the 50-GHz channel is sensitive to the hydrometeors, especially in convective regions, so we can use this independent measurement as an indirect validation. To make a direct comparison with the

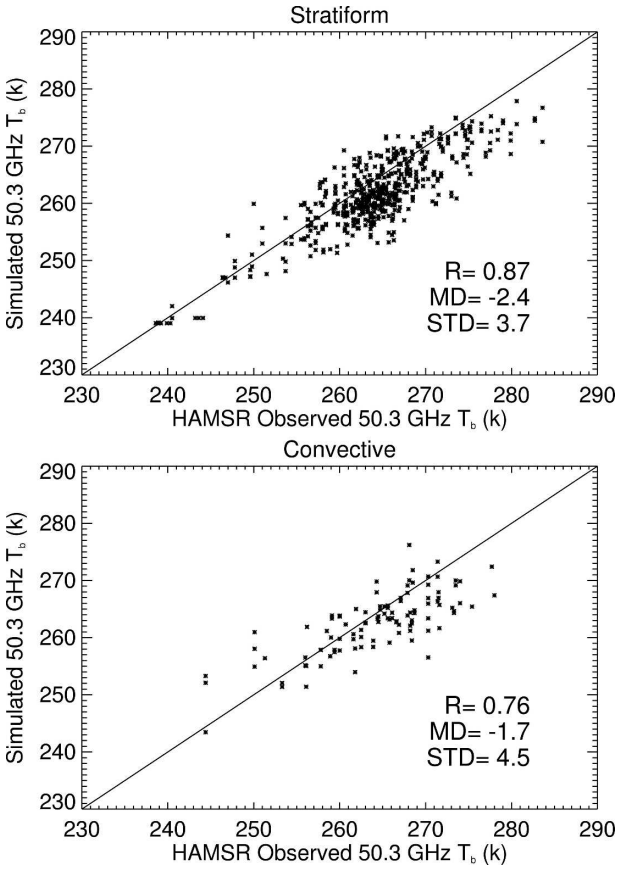

FIG. 10. The comparison between observed and retrieved 50-GHz T_bs for (top) stratiform and (bottom) convective samples.

independent measurement at 50 GHz, we have calculated T_b at 50 GHz (T_b50) from the RTM using as input the set of retrieved hydrometeor profiles and N_0s for the 1019 EDOP–AMPR–HAMSR-matched samples during three Hurricane Erin flights. Figure 10 shows the scatterplot comparison between the observed and retrieved 50-GHz T_bs for stratiform and convective samples. The qualitative agreement is good, because the absolute mean differences are less than 10 K. The mean difference depends on the situation, and is –2.4 K for stratiform regions and –1.7 K for convective regions. The bias is always negative, indicating a weak underestimate of the retrieved T_b50. However, notice that the underestimates are mainly in high brightness temperature regions (greater than 270 K). Checking the dataset, these points are mainly located around the eye region. They might be biased by the uncertainties of the sea surface temperature and wind speed. The standard deviation of the Tb difference is 3.7 K in stratiform regions, and it increases to 4.5 K in convective regions. Again, this is because of uncertainties caused by the snow–graupel fraction assumption in the algorithm.

Nevertheless, the global agreement of the measured and retrieved brightness temperatures at an independent channel allows us to conclude that both the inversion procedure and the retrieved parameters are consistent with the 50-GHz observations.

e. Comparisons of LWC and surface rain-rate retrievals with radar-only and radiometer-only estimates

Above we have compared the retrieved IWC and 50-GHz brightness temperature with independent measurements. The combined radar–radiometer algorithm also has the ability to retrieve the LWC profile and therefore to derive the surface rain rate. However, there are no direct measurements in this CAMEX-4 dataset available to evaluate LWC and rain-rate retrievals. However, radar-only and radiometer-only methods can be compared. Comparisons between different algorithms will help us to understand the advantages and disadvantages of the various algorithms.

The radar-only method to estimate LWC uses the empirical *Z*–LWC relationship given by Willis and Jorgensen (1981), which was derived from aircraft measurements of hurricane raindrop spectra at altitudes of less than 3 km. This relation is for both stratiform and convective regions in hurricanes. Jorgensen and Willis (1982) and Houze et al. (1992) find that in hurricanes, on average the raindrop size distribution is mixed by the strong horizontal winds and that no significant difference exists between stratiform and convective situations. Results described in Jiang et al. (2006) provide the same independent verification of this conclusion.

Figure 11 provides a comparison of LWC retrieved by the combined algorithm and the radar-only method, based on the seven-flight dataset. Frequency plots rather than scatterplots are used, given the large number of points considered in this analysis. The radar–radiometer estimates and radar-only estimates are well correlated. From Fig. 11a, in stratiform regions, there is a systematic overestimation of low-intensity LWC (less than 0.1 g m^{-3}) relative to radar-only estimates by the combined algorithm. From Fig. 11b, in convective regions, an underestimate of the high-intensity LWC by the combined radar–radiometer method is found relative to the radar-only method. A possible reason for this disagreement is the PSD variation for stratiform and convective regions, which is not taken into account in the *Z*–LWC relationship. The nonuniform beamfilling problem (Chiu et al. 1990; Short and North 1990) for the combined algorithm could also cause some underestimation in convective regions because the AMPR's footprint at 10 and 19 GHz is 2.8 km, which is much larger than the EDOP footprint at the surface

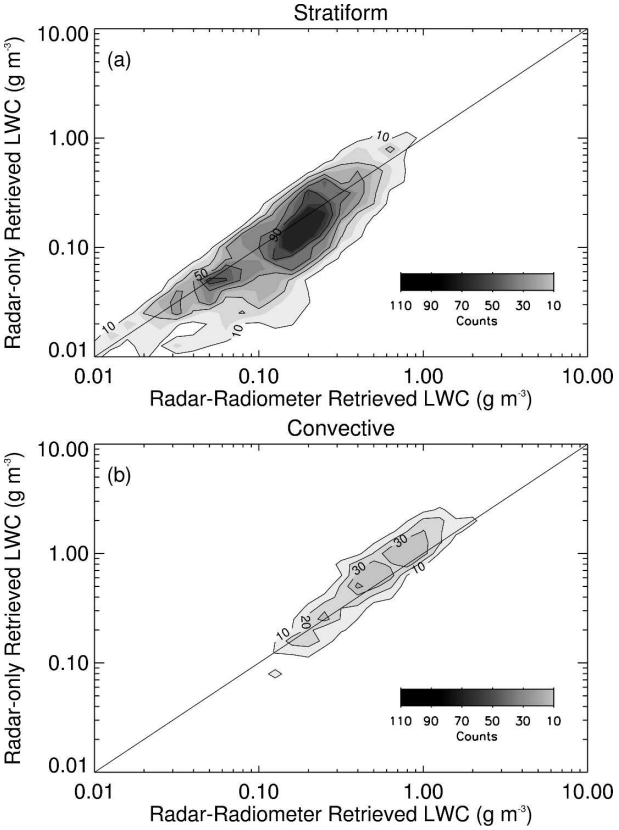

FIG. 11. Frequency plots of radar–radiometer- vs radar-only-retrieved liquid water content for (a) stratiform and (b) convective samples.

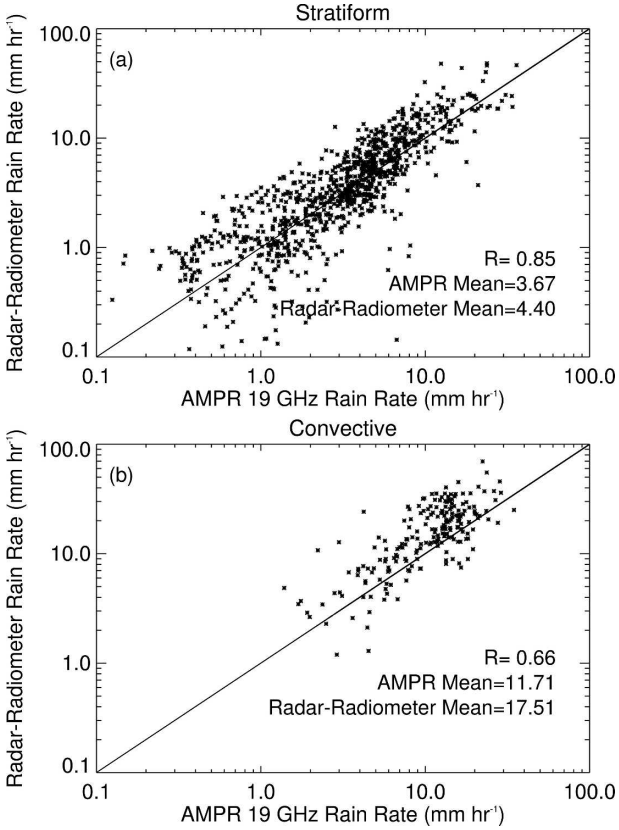

FIG. 12. Comparisons of surface rain rates derived by the emission-based radiometer-only algorithm from AMPR 19-GHz observations (AMPR 19-GHz rain rate) and the combined algorithm from EDOP and AMPR observations (radar–radiometer rain rate) for (a) stratiform and (b) convective regions.

(1.1 km). The mean LWC derived from the combined (radar only) algorithm in stratiform regions is 0.171 (0.166) g m^{-3}, and in convective regions it is 0.593 (0.751) g m^{-3}. The mean values for convective and stratiform regions (0.22 and 0.23 g m^{-3}) are very close to each other.

The emission-based radiometer algorithm developed by Wilheit et al. (1977) has been used in many studies (Adler and Rodgers 1977; Chiu et al. 1990; Shin et al. 1990). This algorithm is not designed to retrieve LWC directly, but to calculate surface rain rate from brightness temperatures at low frequencies. Here we will show the comparison of the rain-rate retrievals by this emission-based radiometer-only algorithm with the combined algorithm developed in this study. The emission-based technique used in this comparison is that of Chiu et al. (1990) based on the 19-GHz brightness temperature observations.

However, direct comparisons cannot be made because the combined algorithm generates liquid water contents while the emission-based method derives the surface rain rates. An equivalent surface rain rate is obtained for the combined retrievals by applying a radar reflectivity–fall speed relationship given by Joss and Waldvogel (1970) at near surface.

Figure 12 shows the comparison of surface rain rates derived by the emission-based radiometer-only algorithm from AMPR 19-GHz observations and the combined algorithm from EDOP and AMPR observations for stratiform and convective regions. These two estimates resemble each other, with correlation coefficients of 0.85 and 0.66 for stratiform and convective regions, respectively. It is also seen that for a rain rate less than 10 mm h^{-1}, the two retrievals are in good agreement. However, for larger rainfall rates, the retrievals from the emission-based radiometer-only method are underestimated relative to the combined algorithm. Possible reasons for the underestimate of AMPR 19-GHz-derived rain rates are that 1) there is a nonuniform beam-filling problem by the radiometer-only algorithm because the footprint for the AMPR 10- and 19-GHz channels is much larger than that for

EDOP, and 2) the radiation at 19 GHz becomes saturated for a rain rate larger than 10–15 mm h^{-1}.

5. Conclusions

A combined radar–radiometer algorithm is developed to retrieve the vertical hydrometeor profiles in tropical cyclones and convective systems over oceans. It has new features when compared with existing combined precipitation algorithms. It is designed to use different N_0s for rain, snow, and graupel to estimate both IWC and LWC profiles. It uses the vertical radar reflectivity profile to constrain the vertical shape of the retrieved hydrometeor profiles and uses the radiometer brightness temperatures to determine the vertically integrated ice and liquid water content, attempting to optimize consistency with both radar and radiometer observations.

The algorithm is applied to the CAMEX-4 tropical cyclones and convection dataset. The retrieved IWC at about 8–11 km is compared with DC-8 aircraft in situ measurements. After minimizing the mismatch problem between the ER-2 and DC-8 aircraft, the agreement is relatively good in stratiform regions. However, in convective regions, the uncertainty is large, although the mean difference between the retrieved and aircraft-derived IWC is very small. We conclude that the assumption of all-snow above the melting layer in stratiform regions is reasonable for tropical oceanic rainfall systems, confirming the same findings from microphysical measurements (Stith et al. 2002; Black and Hallett 1986, 1999). The very simple snow–graupel fraction assumption in convective regions is the main reason for the large IWC uncertainty. Small-scale changes in particle size distributions are another limitation. Sensitivity tests show that the retrievals are relatively insensitive to surface wind speed, environmental temperature and humidity, and cloud water content. However, the potential presence of large amounts of supercooled water in strong convective cores, ignored in this algorithm, would result in underestimates of ice water content in those cores.

An underestimate of IWC at 8–11 km by both the simplified GP algorithm and the radar-only Z–*M* method relative to the combined radar–radiometer algorithm and aircraft in situ measurements is found. The simple microphysics assumption of GP is responsible for the underestimate of simplified GP. It is hypothesized that the *Z*–IWC relation (Black 1990) used here is not suitable for above-7-km altitudes. The retrieved LWC and surface rain rate are in agreement with radar-only and radiometer-only estimates. By comparison with independent measurements, 50-GHz brightness temperature retrievals are also quite reasonable.

Applying the algorithm to TRMM data will generate a valuable database to study the microphysical properties in tropical oceanic rainfall systems and should help to improve microphysical parameterizations in numerical models. The algorithm has been developed based on several assumptions, and thus can be improved with more advanced knowledge concerning the particle size distributions, particle phases, and bulk densities in the ice region. The crucial assumption of snow–graupel–supercooled water fractions in the ice region causes a large uncertainty in convective precipitation and the transition regions. Either more microphysical observations or a better approach is needed to improve the retrieval. For the LWC retrieval in the rain region, the inclusion of the melting layer emission is necessary in order to reduce the overestimate caused by this effect.

Acknowledgments. Andy Heymsfield, Gerry Heymsfield, Aaron Bansemer, Lin Tian, Robbie Hood, and Frank LaFontaine provided assistance in processing microphysics, EDOP, and AMPR data during CAMEX. The authors acknowledge help from Chris Kummerow for providing the microwave radiative transfer model. Thanks are given to Mircea Grecu, Bill Olson, Gail Skofronick-Jackson, and Zhien Wang for their assistance in developing the combined radar–radiometer algorithm. Thanks are given to Gerry Heymsfield, Tim Garrett, Jay Mace, Steve Krueger, Zhaoxia Pu, Cynthia Twohy, Larry Belcher, Dan Cecil, Steve Nesibitt, Baike Xi, Chuntao Liu, Galdino Mota, and Yaping Li for discussion and feedback. The constructive criticisms by the anonymous reviewers led to significant improvements in the manuscript. This research was supported by NASA CAMEX Grant NAG5-10682, NASA TRMM Grant NAG5-9717, and NASA Earth System Science Graduate Fellowship Grant NGT5-30492. The authors thank Ramesh Kakar (NASA headquarters) for his continued support of TRMM and CAMEX science.

REFERENCES

Adler, R. F., and E. B. Rodgers, 1977: Satellite-observed latent heat release in a tropical cyclone. *Mon. Wea. Rev.,* **105,** 956–963.

Black, R. A., 1990: Radar reflectivity-ice water content relationships for use above the melting level in hurricanes. *J. Appl. Meteor.,* **29,** 955–961.

——, and J. Hallett, 1986: Observations of the distribution of ice in hurricanes. *J. Atmos. Sci.,* **43,** 802–822.

——, and ——, 1999: Electrification of the hurricane. *J. Atmos. Sci.,* **56,** 2004–2028.

——, H. B. Bluestein, and M. L. Black, 1994: Unusually strong vertical motions in a Caribbean hurricane. *Mon. Wea. Rev.,* **122,** 2722–2739.

——, G. M. Heymsfield, and J. Hallett, 2003: Extra large particle images at 12 km in a hurricane eyewall: Evidence of high-

altitude supercooled water? *Geophys. Res. Lett.,* **30,** 2124, doi:10.1029/2003GL017864.

Cecil, D. J., and E. J. Zipser, 1999: Relationships between tropical cyclone intensity and satellite-based indicators of inner core convection: 85-GHz ice scattering signature and lightning. *Mon. Wea. Rev.,* **127,** 103–123.

——, ——, and S. W. Nesbitt, 2002: Reflectivity, ice scattering, and lightning characteristics of hurricane eyewalls and rainbands. Part I: Quantitative description. *Mon. Wea. Rev.,* **130,** 769–784.

Chiu, L. S., G. R. North, D. A. Short, and A. McConnell, 1990: Rain estimates from satellite: Effect of the finite field of view. *J. Geophys. Res.,* **95,** 2177–2185.

Ferreira, F., P. Amayenc, S. Oury, and J. Testud, 2001: Study and tests of improved rain estimates from the TRMM precipitation radar. *J. Appl. Meteor.,* **40,** 1878–1899.

Fiorino, S. T., 2002: Investigation of microphysical assumptions in TRMM radiometer's rain profile algorithm using KWAJEX satellite, aircraft and surface datasets. Ph.D. dissertation, The Florida State University, 104 pp.

Goffe, W. L., G. D. Ferrier, and J. Rogers, 1994: Global optimization of statistical functions with simulated annealing. *J. Econ.,* **60,** 65–99.

Grecu, M., and E. N. Anagnostou, 2002: Use of passive microwave observations in a radar rainfall-profiling algorithm. *J. Appl. Meteor.,* **41,** 702–715.

——, W. S. Olson, and E. N. Anagnostou, 2004: Retrieval of precipitation profiles from multiresolution, multifrequency active and passive microwave observations. *J. Appl. Meteor.,* **43,** 562–575.

Haddad, Z. S., E. A. Smith, C. D. Kummerow, T. Iguchi, M. R. Farrar, S. L. Durden, M. Alves, and W. S. Olson, 1997: The TRMM day-1 radar/radiometer combined rain-profiling algorithm. *J. Meteor. Soc. Japan,* **75,** 799–809.

Hallett, J., R. I. Sax, D. Lamb, and A. S. Ramachandra Murty, 1978: Aircraft measurements of ice in Florida cumuli. *Quart. J. Roy. Meteor. Soc.,* **104,** 631–651.

Herman, L. R., and A. J. Heymsfield, 2003: Aircraft icing at low temperatures in Tropical Storm Chantal (2001). *Geophys. Res. Lett.,* **30,** 1955, doi:10.1029/2003GL017746.

Heymsfield, A. J., S. Lewis, A. Bansemer, J. Iaquinta, L. M. Miloshevich, M. Kajikawa, C. Twohy, and M. R. Poellot, 2002a: A general approach for deriving the properties of cirrus and stratiform ice cloud particles. *J. Atmos. Sci.,* **59,** 3–29.

——, A. Bansemer, P. R. Field, S. L. Durden, J. L. Stith, J. E. Dye, W. Hall, and C. A. Grainger, 2002b: Observations and parameterizations of particle size distributions in deep tropical cirrus and stratiform precipitating clouds: Results from in situ observations in TRMM field campaigns. *J. Atmos. Sci.,* **59,** 3457–3491.

——, S. Lewis, S. L. Durden, and T. P. Bui, 2006: Ice microphysics observations in Hurricane Humberto: Comparison with non-hurricane generated ice cloud layers. *J. Atmos. Sci.,* **63,** 288–308.

Heymsfield, G. M., and Coauthors, 1996: The EDOP radar system on the high-altitude NASA ER-2 aircraft. *J. Atmos. Oceanic Technol.,* **13,** 795–809.

——, J. B. Halverson, J. Simpson, L. Tian, and T. P. Bui, 2001: ER-2 Doppler radar investigations of the eyewall of Hurricane Bonnie during the Convective and Moisture Experiment-3. *J. Appl. Meteor.,* **40,** 1310–1330.

Houze, R. A., F. D. Marks Jr., and R. A. Black, 1992: Dual-aircraft investigation of the inner core of Hurricane Norbert. Part II: Mesoscale distribution of ice particles. *J. Atmos. Sci.,* **49,** 943–962.

Iguchi, T., T. Kozu, R. Meneghini, J. Awaka, and K. Okamoto, 2000: Rain-profiling algorithm for the TRMM precipitation radar. *J. Appl. Meteor.,* **39,** 2038–2052.

Jiang, H., 2004: Quantitative precipitation and hydrometeor content estimation in tropical cyclones from remote sensing observations. Ph.D. dissertation, University of Utah, 207 pp.

——, P. G. Black, E. J. Zipser, F. D. Marks, and E. W. Uhlhorn, 2006: Validation of rain-rate estimation in hurricanes from the stepped frequency microwave radiometer: Algorithm correction and error analysis. *J. Atmos. Sci.,* **63,** 252–267.

Jorgensen, D. P., and P. T. Willis, 1982: A *Z-R* relationship for hurricanes. *J. Appl. Meteor.,* **21,** 356–366.

——, and M. A. LeMone, 1989: Vertical velocity characteristics of oceanic convection. *J. Atmos. Sci.,* **46,** 621–640.

——, E. J. Zipser, and M. A. LeMone, 1985: Vertical motions in intense hurricanes. *J. Atmos. Sci.,* **42,** 839–856.

Joss, J., and A. Waldvogel, 1970: Raindrop size distributions and Doppler velocities. Preprints, *14th Conf. on Radar Meteorology,* Tucson, AZ, Amer. Meteor. Soc., 153–156.

——, and E. G. Gori, 1978: Shapes of raindrop size distributions. *J. Appl. Meteor.,* **17,** 1054–1061.

Kakar, R., M. Goodman, R. Hood, and A. Guillory, 2006: Overview of the Convection and Moisture Experiment (CAMEX). *J. Atmos. Sci.,* **63,** 5–18.

Keller, V. W., and R. I. Sax, 1981: Microphysical development of a pulsating cumulus tower: A case study. *Quart. J. Roy. Meteor. Soc.,* **107,** 679–697.

Korolev, A. V., M. P. Bailey, J. Hallett, and G. Isaac, 2004: Laboratory and in situ observation of deposition growth of frozen drops. *J. Appl. Meteor.,* **43,** 612–622.

Kummerow, C., and J. A. Weinman, 1988: Determining microwave brightness temperatures from precipitating horizontally finite and vertically structured clouds. *J. Geophys. Res.,* **93,** 3720–3728.

——, W. S. Olson, and L. Giglio, 1996: A simplified scheme for obtaining precipitation and vertical hydometeor profiles from passive microwave sensors. *IEEE Trans. Geosci. Remote Sens.,* **34,** 1213–1232.

——, and Coauthors, 2000: The status of the Tropical Rainfall Measuring Mission (TRMM) after two years in orbit. *J. Appl. Meteor.,* **39,** 1965–1982.

——, and Coauthors, 2001: The evolution of the Goddard profiling algorithm (GPROF) for rainfall estimation from passive microwave sensors. *J. Appl. Meteor.,* **40,** 1801–1820.

Lambrigtsen, B. H., and A. L. Riley, 2002: Microwave scattering observed in convective cells during CAMEX-4. Preprints, *22d Conf. on Hurricanes and Tropical Meteorology,* San Diego, CA, Amer. Meteor. Soc., 515–516.

LeMone, M. A., and E. J. Zipser, 1980: Cumulonimbus vertical velocity events in GATE. Part I: Diameter, intensity and mass flux. *J. Atmos. Sci.,* **37,** 2444–2457.

Liu, Y., and J. Hallett, 1998: On size distributions of cloud droplets growing by condensation: A new conceptual model. *J. Atmos. Sci.,* **55,** 527–536.

Lord, S. J., H. E. Willoughby, and J. M. Piotrowicz, 1984: Role of a parameterized ice-phase microphysics in an axisymmetric, nonhydrostatic tropical cyclone model. *J. Atmos. Sci.,* **41,** 2836–2848.

Lucas, C., E. J. Zipser, and M. A. LeMone, 1994: Vertical velocity in oceanic convection off tropical Australia. *J. Atmos. Sci.,* **51,** 3183–3193.

Mace, G. G., T. A. Arkerman, P. Minnis, and D. F. Young, 1998: Cirrus layer microphysical properties derived from surface-based millimeter radar and infrared interferometer data. *J. Geophys. Res.,* **103,** 23 207–23 216.

Macklin, W. C., 1962: The density and structure of ice formed by accretion. *Quart. J. Roy. Meteor. Soc.,* **88,** 30–55.

Marshall, J. S., and W. McK. Palmer, 1948: The distribution of raindrops with size. *J. Atmos. Sci.,* **5,** 165–166.

Marzano, F. S., A. Mugnai, G. Panegrossi, N. Pierdicca, E. A. Smith, and J. Turk, 1999: Bayesian estimation of precipitating cloud parameters from combined measurements of spaceborne microwave radiometer and radar. *IEEE Trans. Geosci. Remote Sens.,* **37,** 596–613.

Nesbitt, S. W., E. J. Zipser, and C. D. Kummerow, 2004: An examination of version-5 rainfall estimates from the TRMM Microwave Imager, precipitation radar, and rain gauges on global, regional, and storm scales. *J. Appl. Meteor.,* **43,** 1016–1036.

Olson, W. S., C. D. Kummerow, G. M. Heymsfield, and L. Giglio, 1996: A method for combined passive–active microwave retrievals of cloud and precipitation profiles. *J. Appl. Meteor.,* **35,** 1763–1789.

——, P. Bauer, N. F. Viltard, D. E. Johnson, W.-K. Tao, R. Meneghini, and L. Liao, 2001a: A melting-layer model for passive/active microwave remote sensing applications. Part I: Model formulation and comparison with observations. *J. Appl. Meteor.,* **40,** 1145–1163.

——, ——, C. D. Kummerow, Y. Hong, and W.-K. Tao, 2001b: A melting-layer model for passive/active microwave remote sensing applications. Part II: Simulation of TRMM observations. *J. Appl. Meteor.,* **40,** 1164–1179.

Prasad, N., H.-Y. M. Yeh, R. F. Adler, and W. K. Tao, 1995: Microwave and infrared simulations of an intense convective system and comparison with aircraft observations. *J. Appl. Meteor.,* **34,** 153–174.

Rao, G. V., and P. D. MacArthur, 1994: The SSM/I estimated rainfall amounts of tropical cyclones and their potential in predicting the cyclone intensity changes. *Mon. Wea. Rev.,* **122,** 1568–1574.

Rutledge, S. A., and P. V. Hobbs, 1984: The mesoscale and microscale structure and organization of clouds and precipitation in midlatitude cyclones. XII: A diagnostic modeling study of precipitation development in narrow cold-frontal rainbands. *J. Atmos. Sci.,* **41,** 2949–2972.

Shin, K.-S., P. E. Riba, and G. R. North, 1990: Estimation of area-averaged rainfall over tropical oceans from microwave radiometry: A single channel approach. *J. Appl. Meteor.,* **29,** 1031–1042.

Short, D. A., and G. R. North, 1990: The beam filling error in the Nimbus 5 electronically scanning microwave radiometer observations of Global Atlantic Tropical Experiment rainfall. *J. Geophys. Res.,* **95,** 2187–2193.

Simpson, J., R. F. Adler, and G. R. North, 1988: A proposed Tropical Rainfall Measuring Mission (TRMM) satellite. *Bull. Amer. Meteor. Soc.,* **69,** 278–295.

Simpson, R. H., 1963: Liquid water in squall lines and hurricanes at air temperatures lower than −40°C. *Mon. Wea. Rev.,* **91,** 687–693.

Skofronick-Jackson, G. M., J. R. Wang, G. M. Heymsfield, R. Hood, W. Manning, R. Meneghini, and J. A. Weinman, 2003: Combined radiometer–radar microphysical profile estimations with emphasis on high-frequency brightness temperature observations. *J. Appl. Meteor.,* **42,** 476–487.

Spencer, R. W., R. E. Hood, F. J. Lafontaine, E. A. Smith, R. Platt, J. Galliano, V. L. Griffin, and E. Lobl, 1994: High-resolution imaging of rain systems with the Advanced Microwave Precipitation Radiometer. *J. Atmos. Oceanic Technol.,* **11,** 849–857.

Stith, J. L., J. E. Dye, A. Bansemer, A. J. Heymsfield, C. A. Grainger, W. A. Petersen, and C. Robert, 2002: Microphysical observations of tropical clouds. *J. Appl. Meteor.,* **41,** 97–117.

Tesmer, J. R., and T. T. Wilheit, 1998: An improved microwave radiative transfer model for tropical oceanic precipitation. *J. Atmos. Sci.,* **55,** 1674–1689.

Testud, J., S. Oury, R. A. Black, P. Amayenc, and X. Dou, 2001: The concept of "normalized" distribution to describe raindrop spectra: A tool for cloud physics and cloud remote sensing. *J. Appl. Meteor.,* **40,** 1118–1140.

Tian, L., G. M. Heymsfield, and R. C. Srivastava, 2002: Measurement of attenuation with airborne and ground-based radar in convective storms over land and its microphysical implications. *J. Appl. Meteor.,* **41,** 716–733.

Toracinta, E. R., D. J. Cecil, E. J. Zipser, and S. W. Nesbitt, 2002: Radar, passive microwave, and lightning characteristics of precipitating systems in the Tropics. *Mon. Wea. Rev.,* **130,** 802–824.

Viltard, N., E. Obligis, V. Marecal, and C. Klapisz, 1998: Retrieval of precipitation from microwave airborne sensors during TOGA COARE. *J. Appl. Meteor.,* **37,** 701–717.

——, C. Kummerow, W. S. Olson, and Y. Hong, 2000: Combined use of the radar and radiometer of TRMM to estimate the influence of drop size distribution on rain retrievals. *J. Appl. Meteor.,* **39,** 2103–2114.

Vivekanandan, J., J. Turk, and V. N. Bringi, 1991: Ice water path estimation and characterization using passive microwave radiometry. *J. Appl. Meteor.,* **30,** 1407–1421.

Wang, Z., and K. Sassen, 2002: Cirrus cloud microphysical property retrieval using lidar and radar measurements. Part I: Algorithm description and comparison with in situ data. *J. Appl. Meteor.,* **41,** 218–229.

Wilheit, T. T., A. T. C. Chang, M. S. V. Rao, E. B. Rodgers, and J. S. Theon, 1977: A satellite technique for quantitatively mapping rainfall rates over the oceans. *J. Appl. Meteor.,* **16,** 551–560.

——, ——, and L. S. Chiu, 1991: Retrieval of monthly rainfall indices from microwave radiometric measurements using probability distribution functions. *J. Atmos. Oceanic Technol.,* **8,** 118–136.

Willis, P. L., and D. P. Jorgensen, 1981: Reflectivity relationships for hurricanes. Preprints, *20th Conf. on Radar Meteorology,* Boston, MA, Amer. Meteor. Soc., 199–200.

Zipser, E. J., and M. A. LeMone, 1980: Cumulonimbus vertical velocity events in GATE. Part II: Synthesis and model core structure. *J. Atmos. Sci.,* **37,** 2458–2469.

——, and K. R. Lutz, 1994: The vertical profile of radar reflectivity of convective cells: A strong indicator of storm intensity and lightning probability? *Mon. Wea. Rev.,* **122,** 1751–1759.